Theor Chem Account (2008) 121:313–319
DOI 10.1007/s00214-008-0480-1

REGULAR ARTICLE

Regioselectivity preference of testosterone hydroxylation by cytochrome P450 3A4

Yan Zhang · Phani Morisetti · Jeffery Kim · Lynelle Smith · Hai Lin

Received: 30 April 2008 / Accepted: 2 September 2008 / Published online: 18 September 2008

Abstract Theoretical studies are presented into the experimentally observed regioselectivity difference of testosterone hydroxylation by cytochrome P450 3A4 at the 1β, 2β, 6β, and 15β positions. Such regioselectivity is investigated by density functional theory calculations on a model system. The barrier heights of hydrogen abstraction, which are corrected by zero-point vibrational energies, are computed to be about 10.1, 13.6, 14.4, and 16.2 kcal/mol for the 6β-, 2β-, 15β-, and 1β-positions, respectively. The calculated barriers suggest the regioselectivity preference of $6\beta \gg 2\beta > 15\beta > 1\beta$, which is in good agreement with experimental findings.

Keywords Cytochrome P450 3A4 · Testosterone hydroxylation · Regioselectivity · Density functional theory

1 Introduction

The cytochrome P450 [1, 2] super-family of ubiquitous heme-containing proteins is involved in the metabolism of exogenous and endogenous compounds including steroids and drugs. The human P450 3A4 enzyme, which is one of the most abundant P450 proteins in the human liver and small intestine, [3, 4] has a wide range of the substrate specificity and metabolizes nearly 50% of the drugs used today [5]. Testosterone metabolism is a prototypical reaction of P450 3A4. Testosterone is a major androgen primarily secreted by the testes of males and the ovaries of females, and it plays a key role in human health and well-being. In human liver microsomes, testosterone is primarily metabolized by P450 3A4, and hydroxylation is the principal pathway of its oxidative metabolism. Experiments have revealed that the hydroxylation of testosterone leads to four major products: 6β-, 2β-, 1β-, and 15β-hydroxytestosterone (Scheme 1) [6, 7]. The reaction rates of these products were determined to be in the order $6\beta \gg 2\beta > 15\beta > 1\beta$, with the difference between 15β and 1β being very small [7].

It is of interest to ask why P450 3A4 displays such regioselectivity preference of testosterone hydroxylation. The present study investigates this problem from the computational point of view. In the consensus abstraction-rebound mechanism [8] shown in Scheme 2, the C–H bond hydroxylation is initiated by hydrogen abstraction by the active oxidant, the iron-oxo porphyrin π-cation species named compound I (Cpd I) [9]. The resulting intermediate complex (2) consists of a carbon radical and an iron-hydroxo species, which recombine to yield an alcohol-ferric product complex (4) in the subsequent rebound step. Focusing on the bacterial P450cam that hydroxylates camphor but also on other systems, theoretical calculations have been carried out to elucidate the electronic structure [10–17] of the oxidant compound I as well as to investigate the hydroxylation pathways [18–25]. These computations include both quantum-mechanical calculations on model systems and hybrid quantum-mechanical/molecular-mechanical [26–31] (QM/MM) studies that consider the

Electronic supplementary material The online version of this article (doi:10.1007/s00214-008-0480-1) contains supplementary material, which is available to authorized users.

Y. Zhang · P. Morisetti · J. Kim · L. Smith · H. Lin (✉)
Chemistry Department, University of Colorado Denver,
PO Box 173364, Denver, CO 80217, USA
e-mail: hai.lin@ucdenver.edu

Present Address:
J. Kim
Rush University Medical College,
Chicago, IL 60612, USA

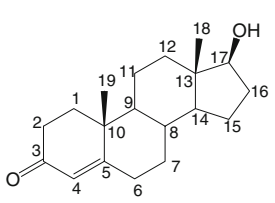

	Sample Reaction Rate (min^{-1})
1β-hydroxy	4.8 ± 0.1
2β-hydroxy	11 ± 0.1
6β-hydroxy	83 ± 1
15β-hydroxy	5.0 ± 0.1

Scheme 1 Testosterone and its hydroxylation in human liver microsomes, where the kinetic parameters were taken from Ref. [7]

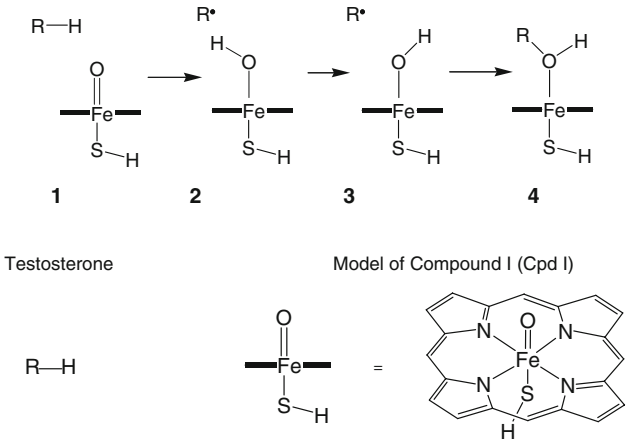

Scheme 2 Model of the abstraction-rebound mechanism for testosterone hydroxylation by P450

protein-solvent environment. The QM/MM studies confirm the conclusions drawn from the QM gas-phase model computations. A very recent review by Shaik, Thiel, and coworkers [32] provides a detailed overview of the extensive theoretical investigations on P450 enzymes. Notably, a two-state reactivity (TSR) scenario [18, 33] has been proposed that invokes reactions on the potential energy surfaces of two spin-states, a low-spin (doublet) state and a high-spin (quartet) state. Both spin states have similar barriers for the hydrogen abstraction step, which is rate-limiting in the abstraction-rebound mechanism. On the other hand, the rebound on the doublet spin state is almost without a barrier, leading to effective concerted reaction, whereas the quartet state experiences a significant barrier for recombination, which leads to a truly stepwise reaction. The coupling [34] between two reaction pathways on the doublet and quartet spin states rationalizes, in the framework of the abstraction-rebound mechanism, the seemingly contradictory findings in the radical-clock experiments [35, 36]. The TSR scenario has been generalized to a multi-state reactivity (MSR) scenario [37, 38].

In the present contribution, we perform density functional theory (DFT) model calculations for testosterone hydroxylation by P450 3A4. We concentrate on the rate-limiting H-abstraction step, i.e., the step that converts Structure 1 to Structure 2 in Scheme 2, and search for the transition states for both doublet and quartet spin states, in accordance with the TSR scenario.

2 Methods

Cpd I was modeled as an iron-oxo-porphyrin complex without side chains (Scheme 2), whose geometry was taken from the crystal structure 2V0M [39] with the oxo atom and hydrogen atoms being added. The proximal cysteinate ligand was truncated to HS^-, as suggested by Ogliaro et al. [12] All calculations were performed using the B3LYP [40–42] density functional model and the *Gaussian03* [43] program package. For the geometry optimization we employed the effective core potential coupled with the double-ζ LACVP basis [44] for iron and a 6-31G basis [45, 46] for the other atoms; such a basis set combination is abbreviated as B1. The relaxed scans of potential energy surfaces for hydrogen abstractions at the 1β, 2β, 6β, and 15β positions were carried out. In the scans, the active O_{oxo}–H_{trans} bond distance (O_{oxo} is the oxygen atom bonded to iron, and H_{trans} is the hydrogen atom being transferred) was constrained to certain values, while the other degrees of freedom were optimized. Based on the scanned energy profiles, transition structures were optimized and were characterized by normal-mode vibrational analysis. Visualization of the single imaginary normal modes confirmed that the transition structures were correct. The reactive complexes (1) and the intermediate complexes after hydrogen abstraction (2) were also fully optimized.

At B1 optimized geometries, we also performed single-point calculations with an improved basis set combination denoted B2, which assigns a larger 6–31++G** basis set [45–49] to selected atoms. Those selected atoms are the six atoms coordinated to iron (four nitrogen atoms, an oxygen atom, and a sulfur atom), the four reactive carbon atoms (C^1, C^2, C^6, and C^{15}) of testosterone, and the eight hydrogen atoms bonded to those reactive carbon atoms. Zero-point vibrational energies (ZPVE) were calculated at the B1 level assuming harmonic vibrations at the stationary geometries.

The widely used Wigner tunneling [50] coefficient κ_W was also computed as

$$\kappa_W = 1 + (1/24)\left|\nu^{\ddagger}/k_B T\right|^2 \quad (1)$$

where $\nu^{\ddagger}$ is the imaginary frequency at the conventional transition state. Here, we remind readers that the Wigner tunneling coefficient must be interpreted with caution, a point that is sometimes overlooked. The reason is that $|\nu^{\ddagger}| \ll k_B T$ is required for the calculations of Wigner tunneling coefficient to converge; at near room temperatures

this requires $|v^{\ddagger}| \ll 200\ \mathrm{cm}^{-1}$, which is not always satisfied (and indeed not satisfied here). Therefore, the Wigner tunneling calculations should be considered as instructive only.

Another one-dimensional tunneling model by Skodje-Truhlar (STR) [51] was employed in the present study. The divergence-free STR model also approximates the barrier by an inversed parabola, in that it is similar to the Wigner tunneling treatment; but the STR method has a wider range of validity. The details of the STR method can be found in [51, 52] and therefore are not repeated here. We used the imaginary frequencies computed at the optimized transition structures in the STR calculations, where the barrier heights were taken to be with respect to the reactive complexes.

The C–H bond dissociation energy was computed as the difference between the energy of testosterone and the summed energy of the hydrogen and the testosterone radical (after the hydrogen abstraction for each position), where the geometries of testosterone and the radicals are fully relaxed.

3 Results

Table 1 summarizes the calculated energy profile for the hydrogen abstractions. The zero of energy was set to the reactant quartet state where the testosterone and Cpd I are well separated. The scanned energy surfaces were plotted as functions of the constrained O_{oxo}–H_{trans} bond distance in the Fig. S1 of the electronic supplementary material. For each spin-state in the 1β, 2β, and 6β cases we found two species of the intermediate complex (2) possessing Fe^{III} and Fe^{IV} characters, respectively. In the case of 15β, we only obtained the Fe^{IV} species despite an extensive search. Filatov et al. [53] suggests that the Fe^{IV} species has a lower energy in the gas phase. In our B1 calculations, the Fe^{III} species are slightly higher ($\leq$2.5 kcal/mol) in energy than the Fe^{IV} species. In the improved B2 calculations the energy difference between the Fe^{III} and Fe^{IV} species are getting smaller (1.5 kcal/mol or less), and in the doublet state of 1β and both spin states of 6β, the relative energy order is even reversed.

As can be seen from Table 1, the energy surfaces of the doublet and quartet spin states are nearly degenerate. The similar energy barrier heights (Table 2) calculated for both the doublet and quartet spin states agree with the two-state reactivity scenario [18, 33]. Going from the B1 calculations to the B2 calculations, the reaction barrier heights change insignificantly (all less than 1.6 kcal/mol and generally within 1 kcal/mol). The presumably more accurate B2 calculations yielded the lowest energy barrier (10.1 kcal/mol) for the 6β-hydrogen abstraction. The barriers are considerably lower than those for the 2β-hydrogen abstractions (13.6 kcal/mol), 15β-hydrogen abstractions (14.4 kcal/mol), and for the 1β-hydrogen abstractions (16.2 kcal/mol).

Figure 1 displays the key geometric data for the transition structures for the 1β-, 2β-, 6β-, and 15β-hydrogen abstractions. All transition structures show almost linear arrangements for the $C' \cdots H_{trans} \cdots O_{oxo}$ moiety, where H_{trans} is transferred between C' and O_{oxo}. The $O_{oxo} \cdots H_{trans}$ distance of the transition structure increases in the order of 1β $\rightarrow$ 15β $\rightarrow$ 2β $\rightarrow$ 6β, while the $C' \cdots H_{trans}$ distance

Table 1 Reaction energy profile corrected by zero-point vibrational energies (in kcal/mol) for hydrogen abstraction at the 1β, 2β, 6β, and 15β positions of testosterone by Compound I

		RH + Cpd I	C_R	TS_H	$C_I(Fe^{IV})$	$C_I(Fe^{III})$
1β	^{2}A	0.1/0.0	−3.9/−4.8	13.2/11.4	8.0/4.1	8.8/3.8
	^{4}A	0.0/0.0	−4.1/−4.9	13.2/13.0	8.2/4.1	9.4/5.0
2β	^{2}A	0.1/0.0	−5.5/−5.4	9.2/9.7	−5.0/−7.6	−2.9/−6.8
	^{4}A	0.0/0.0	−5.5/−5.3	9.0/8.2	−5.0/−7.5	−2.5/−6.3
6β	^{2}A	0.1/0.0	−4.5/−4.8	5.4/5.3	−10.9/−14.0	−10.9/−15.5
	^{4}A	0.0/0.0	−4.4/−4.5	5.1/6.1	−10.9/−14.2	−10.2/−14.8
15β	^{2}A	0.1/0.0	−4.6/−4.7	11.3/9.7	7.2/3.1	n/a
	^{4}A	0.0/0.0	−4.6/−3.8	11.9/11.6	7.4/3.4	n/a

The relative energies are given for B1/B2 calculations. Zero-point vibrational energies are computed at the B1 level. RH + Cpd I denotes the reactant state (where testosterone and Compound I are well-separated), C_R the reactive complex, TS_H the transition state of hydrogen abstraction, C_I the intermediate complex resulted from the hydrogen abstraction, and ^{2}A and ^{4}A label the doublet and quartet spin states, respectively

Table 2 Reaction energy barrier corrected by zero-point vibrational energies (BH, in kcal/mol), imaginary frequency vibrational mode at the saddle point ($v^{\ddagger}$ in cm^{-1}), Wigner tunneling coefficient (κ_W), Skodje-Truhlar tunneling coefficients (κ_{STR}), and bond dissociation energy corrected by zero-point vibrational energies (BDE in kcal/mol) for hydrogen abstraction at the 1β, 2β, 6β, and 15β positions of testosterone by Compound I

		BH	$v^{\ddagger}$	κ_W	κ_{STR}	BDE
1β	^{2}A	17.3/16.2	1324i	2.7	13	94.0
	^{4}A	17.5/17.9	1586i	3.4	71	94.0
2β	^{2}A	14.9/15.1	1686i	3.7	1,264	85.6
	^{4}A	14.8/13.6	1674i	3.7	638	85.6
6β	^{2}A	10.0/10.1	1616i	3.5	125	76.0
	^{4}A	9.6/10.6	1665i	3.7	205	76.0
15β	^{2}A	16.0/14.4	1261i	2.5	9	93.6
	^{4}A	16.6/15.4	1535i	3.3	46	93.6

The barrier heights energies are given for B1/B2 calculations and are with respect to the reactive complexes. Vibrational frequencies and bond dissociation energies are calculated at the B1 level. ^{2}A and ^{4}A label the doublet and quartet spin states, respectively. The temperature was 300 K in the calculations of tunneling coefficients

expresses the opposite trend. In other words, the transition structures resemble the reactant in the increasing order of $6\beta \rightarrow 2\beta \rightarrow 15\beta \rightarrow 1\beta$; this trend correlates well with the exothermicity of the hydrogen abstractions (Table 1) at the four positions, and can be readily rationalized using Hammond's Postulate [54]. Another notable structural feature is the large change in the C^4=C^5 bond distance during the 6β-hydrogen abstraction, which increases from the reactant complex at 1.356 Å through the transition structure to the intermediate complex where the C^4=C^5 is 1.414 Å. A similar but smaller increase in the C^3=O bond distance of testosterone was observed in the 2β-hydrogen abstraction from 1.255 Å in the reactant complex to 1.285 Å in the intermediate complex. For the abstraction at 1β and 15β, those two double bonds do not show notable changes in bond length.

It is natural to ask why the barrier height in the 6β-hydrogen abstraction is much lower than in the other three (1β-, 2β-, and 15β-). The reason for this is that electron delocalization in the 6β case significantly stabilizes the transition structure, and leads to a lower barrier. More specifically, when the 6β-hydrogen transfers to the O_{oxo} atom, an unpaired electron left on the C^6 atom couples with the π electrons of the C^4=C^5 bond, leading to a resonance hybrid represented by two resonance structures, C^4–C^5=C^6 and C^4=C^5–C^6. This is evident from the similar bond distances $r(C^4–C^5) = 1.414$ Å and $r(C^5–C^6) = 1.385$ Å in the intermediate complex (2). It is also evident from the smeared spin density on the C^4 (−0.573/0.574 e), C^5 (0.253/−0.253 e), and C^6 (−0.548/0.548 e) atoms, where the spin densities are given as doublet/quartet state in the parentheses (see Table 3). The resonance described above significantly stabilizes the product of the hydrogen abstraction and leads to a great amount of exothermicity as well. The stabilization effect is much smaller in the 2β-hydrogen abstraction, because the oxygen in the C^3=O double bond is very electronegative and attracts the majority of the electron cloud. As for the 1β- and 15β-hydrogen abstractions, no resonance stabilization occurs, and they have the highest barrier heights.

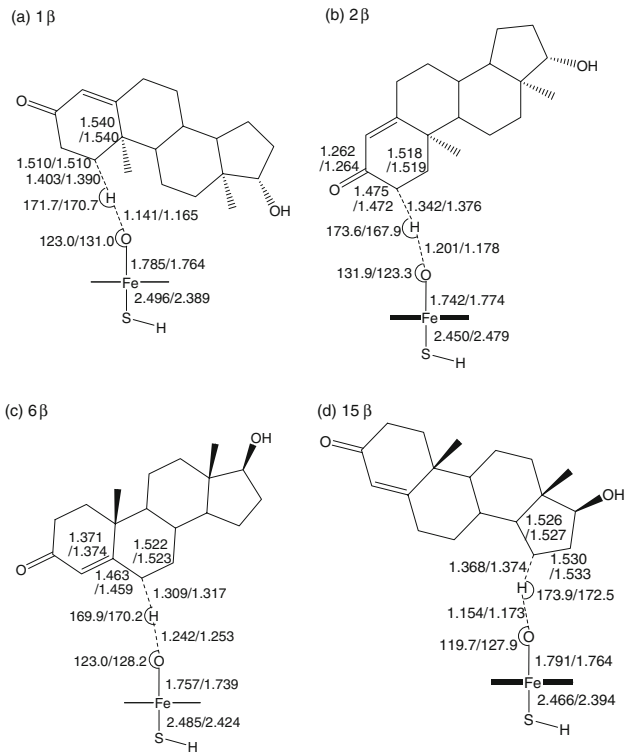

Fig. 1 Transition structures optimized for hydrogen abstractions of testosterone at the **a** 1β, **b** 2β, **c** 6β, and **d** 15β positions. The geometric data are given as $^2A/^4A$. Distances are in Å, and angles in deg. For testosterone, only the hydrogen atoms being transferred are shown

4 Discussion

Assuming that the above four positions of testosterone are all (approximately) equally reachable for hydroxylation in the enzyme active site, one will expect that reaction rates are in the order $6\beta \gg 2\beta > 15\beta > 1\beta$ according to the calculated barriers; this regioselectivity is in agreement with the experimental findings (see also Fig. S3 in the Supporting Information) [7]. On the other hand, we note that the variation of 6 kcal/mol (10–16 kcal/mol) in the calculated barriers seems too large, as the experimental reaction rates differ by less than a factor of 20, which corresponds to a change of about 2 kcal/mol in the reaction barriers based on the transition state theory (assuming the partition functions of the transition state and the tunneling coefficients are the same for all reaction paths).

There are several possible reasons for the deviations in the effective barrier heights. The first possibility is that the calculated barriers are not sufficiently accurate at the employed level of theory. The efficient DFT method was selected due to the considerably large size of the system (89 atoms), and it is very challenging to determine barrier heights to an accuracy of 1 kcal/mol or better. This makes the quantitative agreement in the reaction rates very difficult to achieve. The determination of reaction rates is further complicated by the likelihood of the involvement of hydrogen tunneling at the mild physiological temperature at which these abstractions occur. The experiments by Krauser and Guengerich [55] have implicated the involvement of the quantum tunneling in this situation. The large Wigner tunneling coefficients (2.5–3.7) and Skodje-Truhlar (STR) tunneling coefficients (9–1,264) estimated in Table 2 also imply that quantum tunneling may be significant. As mentioned earlier, the Wigner tunneling treatment is not reliable here because the imaginary frequencies are much larger

Table 3 Spin densities (in e) of selected atoms/groups for stationary structures calculated at the B1 level for the hydrogen abstractions at the 1β, 2β, 6β, and 15β positions of testosterone by Compound I

		$^{2}C_R$	$^{2}TS_H$	$^{2}C_I(Fe^{III})$	$^{2}C_I(Fe^{IV})$	$^{4}C_R$	$^{4}TS_H$	$^{4}C_I(Fe^{III})$	$^{4}C_I(Fe^{IV})$
1β	S	−0.611	−0.502	−0.455	0.002	0.557	0.380	0.444	0.046
	Fe	1.214	1.005	1.019	1.841	1.084	1.318	0.898	1.817
	O_{oxo}	0.882	0.480	0.072	0.249	0.939	0.635	0.212	0.285
	C^1	0.004	0.559	0.998	−0.985	0.004	0.569	1.016	0.993
	Por[a]	−0.528	−0.502	−0.625	−0.128	0.454	0.123	0.515	−0.118
	H_{trans}	−0.002	−0.054	0.003	−0.012	−0.002	−0.037	−0.002	0.015
2β	S	−0.591	−0.317	−0.467	−0.009	0.529	0.398	0.448	−0.012
	Fe	1.222	1.872	0.992	1.808	1.090	0.940	0.848	1.809
	O_{oxo}	0.878	0.177	0.080	0.325	0.934	0.627	0.193	0.325
	C^2	0.002	−0.354	0.817	−0.819	0.003	0.483	0.818	0.821
	Por[a]	−0.549	−0.375	−0.638	−0.127	0.481	0.599	0.555	−0.127
	C^3	−0.000	0.068	−0.138	0.130	−0.003	−0.073	−0.138	−0.131
	O[b]	−0.001	−0.118	0.335	−0.319	0.002	0.142	0.337	0.322
	H_{trans}	−0.001	0.022	−0.007	0.004	−0.001	−0.073	−0.008	−0.003
6β	S	−0.616	−0.456	−0.437	−0.003	0.561	0.423	0.429	0.015
	Fe	1.227	1.089	1.020	1.869	1.095	1.202	0.876	1.853
	O_{oxo}	0.871	0.581	0.063	0.249	0.928	0.691	0.171	0.256
	C^6	0.002	0.323	0.543	−0.548	0.003	0.345	0.551	0.548
	Por[a]	−0.525	−0.593	−0.659	−0.132	0.451	0.284	0.577	−0.115
	C^4	0.001	0.182	0.559	−0.573	0.001	0.242	0.566	0.574
	C^5	−0.000	−0.128	−0.244	0.253	−0.001	−0.150	−0.247	−0.253
	H_{trans}	−0.001	−0.061	−0.004	0.000	−0.001	−0.047	−0.006	0.003
15β	S	−0.619	−0.434	n/a	0.005	0.566	0.415	n/a	0.055
	Fe	1.204	1.035	n/a	1.836	1.074	1.268	n/a	1.808
	O_{oxo}	0.893	0.469	n/a	0.243	0.949	0.643	n/a	0.284
	C^{15}	0.000	0.511	n/a	−0.992	0.000	0.583	n/a	1.006
	Por[a]	−0.520	−0.556	n/a	−0.130	0.445	0.143	n/a	−0.115
	H_{trans}	−0.001	−0.053	n/a	−0.017	−0.001	−0.038	n/a	0.018

[n] C_R is the reactive complex, $^{n}TS_H$ is the transition state of hydrogen abstraction, and $^{n}C_I(Fe^{III})/^{n}C_I(Fe^{IV})$ is the intermediate complex of Fe^{III}/Fe^{IV} character resulted from the hydrogen abstraction, where $n = 2$ and $n = 4$ label the doublet and quartet spin states, respectively. The oxygen bonded to iron is labeled O_{oxo}, the hydrogen being transferred is labeled H_{trans}

[a] Porphyrin

[b] Oxygen atom bonded to C^3 of the testosterone

than k_BT. Our STR calculations likely overestimated the tunneling contribution. Improved STR calculations might be done by employing effective frequencies obtained from parabolic fit to the barrier regions that contribute most to the tunneling coefficients [51, 52]; but that requires information along the reaction path rather than just at the transition state. The difficulties encountered by the two simple one-dimensional tunneling models suggest that more reliable evaluation of quantum tunneling should be done by employing more advanced dynamics theories such as the variational transition state theory with multi-dimensional tunneling [56], which takes into account reaction-path curvature [57] (the coupling between the motion along the reaction coordinate and the generalized normal modes transverse to the reaction coordinate). In view of the size of the model system, direct dynamics [58] calculations where potential energy surfaces are computed on the fly are very difficult; the recently developed and improved multi-configuration molecule mechanics [59–66] method could be a good choice.

Another possibility is the solvent effects that were not accounted for in the present study. Even though the active site is well buried in the P450 3A4, the polarization due to the surroundings could be substantial. An example is the stabilization of the porphyrin-centered radical over the sulfur-centered radical in the determination of the electronic structure of the Cpd I in P450cam [14], whose active site is also well buried. However, as shown in previous

implicit-solvation model computations [67] and explicit QM/MM computations on P450 enzymes [14, 16, 22, 23, 68], the polarization by the protein-solvent environment tends to favor electronic states whose unpaired electrons are highly delocalized more than electronic states whose unpaired electrons are mainly localized. This makes sense, since delocalized electrons are more easily affected by external electric field than localized electrons. For the same reason, one would expect that the relative order of the reaction rates, $6\beta \gg 2\beta > 15\beta > 1\beta$ will be further enforced by the protein-solvent environment, because the delocalization of the unpaired electron in testosterone radical follows this same trend. A definite answer to this question requires a comprehensive investigation employing more realistic solvation models, including implicit and explicit (QM/MM) solvation models.

The third possible reason for the seemingly too large variation in the barrier heights is the assumption that the above four positions of testosterone are all equally reachable for hydroxylation in the enzyme active site. Given the relatively large space of the active site [39, 69, 70], such an assumption seems reasonable. In fact, our very preliminary result (not shown) of docking simulations employing rigid protein geometries are in line with this assumption. However, it is conceivable that the protein is flexible, and the conformational change of the protein will likely affect the testosterone binding which would enhance the preference of certain carbon positions. The unequal availability of the positions for hydroxylation will have a significant effect on the experimental measurements and lead to the deviation in the effective barrier heights from theoretical predictions based on model systems. Docking simulations with the protein flexibility taken into account are currently being carried out in our group as an effort to test this hypothesis.

Not surprisingly, the bond dissociation energy (Table 2) correlates well with the barrier heights of hydrogen abstraction: $6\beta < 2\beta < 15\beta < 1\beta$. Just like de Visser et al. [71], we found that a linear fit was obtained for the ZPVE-corrected barrier heights (averaged over both doublet and quartet spins states) versus the ZPVE-corrected bond dissociation energies (see Fig. S2 in the electronic supplementary material). Even though we have only four data points, the linear correlation is evident. Those bond dissociation energies, together with the other geometric and energetic data computed in this work, will be helpful in further exploration of the structure-reactivity relationship for P450 enzymes [71–74].

Acknowledgments This research is supported by the Research Corporation. We thank the National Cancer Institute-Frederick Advanced Biomedical Computing Center for providing CPU time and access to the *Gaussian03* program. We thank Dr. Hoyt Meyer for critically reading the manuscript.

References

1. Coon MJ (2005) Annu Rev Pharmacol Toxicol 45:1. doi:10.1146/annurev.pharmtox.45.120403.100030
2. Ortiz de Montellano PR (2005) In: Ortiz de Montellano PR (ed) Kluwer/Plenum, New York
3. Guengerich FP (1999) Annu Rev Pharmacol Toxicol 39:1. doi:10.1146/annurev.pharmtox.39.1.1
4. Guengerich FP (2005) Montellano Od (ed) In: Cytochrome P450: structure, mechanism and biochemistry. Kluwer/Plenum, New York, pp 377
5. Evans WE, Relling MV (1999) Science 286:487. doi:10.1126/science.286.5439.487
6. Waxman DJ, Attisano C, Guengerich FP, Lapenson DP (1988) Arch Biochem Biophys 263:424. doi:10.1016/0003-9861(88)90655-8
7. Krauser JA, Voehler M, Tseng L-H, Schefer AB, Godejohann M, Guengerich FP (2004) Eur J Biochem 271:3962. doi:10.1111/j.1432-1033.2004.04339.x
8. Groves JT, McClusky GA (1976) J Am Chem Soc 98:859. doi:10.1021/ja00419a049
9. Groves JT, Watanabe Y (1988) J Am Chem Soc 110:8443. doi:10.1021/ja00233a021
10. Green MT (1999) J Am Chem Soc 121:7939. doi:10.1021/ja991541v
11. Loew GH, Harris DL (2000) Chem Rev 100:407. doi:10.1021/cr980389x
12. Ogliaro F, Cohen S, Filatov M, Harris N, Shaik S (2000) Angew Chem Int Ed Engl 39:3851. doi:10.1002/1521-3773(20001103)39:21<3851::AID-ANIE3851>3.0.CO;2-9
13. Ohta T, Matsuura K, Yoshizawa K, Morishima I (2000) J Inorg Biochem 82:141. doi:10.1016/S0162-0134(00)00162-8
14. Schöneboom JC, Lin H, Reuter N, Thiel W, Cohen S, Ogliaro F et al (2002) J Am Chem Soc 124:8142. doi:10.1021/ja026279w
15. Guallar V, Baik M-H, Lippard SJ, Friesner RA (2003) Proc Natl Acad Sci USA 100:6998. doi:10.1073/pnas.0732000100
16. Bathelt CM, Zurek J, Mulholland AJ, Harvey JN (2005) J Am Chem Soc 127:12900. doi:10.1021/ja0520924
17. Schöneboom JC, Neese F, Thiel W (2005) J Am Chem Soc 127:5840. doi:10.1021/ja0424732
18. Harris N, Cohen S, Filatov M, Ogliaro F, Shaik S (2000) Angew Chem Int Ed 39:2003. doi:10.1002/1521-3773(20000602)39:11<2003::AID-ANIE2003>3.0.CO;2-M
19. Kamachi T, Yoshizawa K (2003) J Am Chem Soc 125:4652. doi:10.1021/ja0208862
20. Park JY, Harris D (2003) J Med Chem 46:1645. doi:10.1021/jm020538a
21. Guallar V, Friesner RA (2004) J Am Chem Soc 126:8501. doi:10.1021/ja036123b
22. Schöneboom JC, Cohen S, Lin H, Shaik S, Thiel W (2004) J Am Chem Soc 126:4017. doi:10.1021/ja039847w
23. Altun A, Guallar V, Friesner RA, Shaik S, Thiel W (2006) J Am Chem Soc 128:3924. doi:10.1021/ja058196w
24. Bach RD, Dmitrenko O (2006) J Am Chem Soc 128:1474. doi:10.1021/ja052111+
25. Wang Y, Wang H, Wang Y, Yang C, Yang L, Han K (2006) J Phys Chem B 110:6154. doi:10.1021/jp060033m
26. Warshel A, Levitt M (1976) J Mol Biol 103:227. doi:10.1016/0022-2836(76)90311-9
27. Lin H, Truhlar DG (2007) Theor Chem Acc 117:185. doi:10.1007/s00214-006-0143-z
28. Senn HM, Thiel W (2007) Top Curr Chem 268:173. doi:10.1007/128_2006_084
29. Singh UC, Kollman PA (1984) J Comput Chem 5:129. doi:10.1002/jcc.540050204

30. Gao J, Thompson MA (eds) (1998) Combined quantum mechanical and molecular mechanical methods: ACS symposium series 712. American Chemical Society, Washington
31. Field MJ, Bash PA, Karplus M (1990) J Comput Chem 11:700. doi:10.1002/jcc.540110605
32. Shaik S, Kumar D, de Visser SP, Altun A, Thiel W (2005) Chem Rev 105:2279. doi:10.1021/cr030722j
33. Shaik S, Filatov M, Schröder D, Schwarz H (1998) Chem Eur J 4:193. doi:10.1002/(SICI)1521-3765(19980210)4:2<193::AID-CHEM193>3.0.CO;2-Q
34. Kumar D, de Visser SP, Shaik S (2003) J Am Chem Soc 125:13024. doi:10.1021/ja036906x
35. Newcomb M, Toy PH (2000) Acc Chem Res 33:449. doi:10.1021/ar960058b
36. Newcomb M, Aebisher D, Shen R, Chandrasena REP, Hollenberg PF, Coon MJ (2003) J Am Chem Soc 125:6064. doi:10.1021/ja0343858
37. de Visser SP, Ogliaro F, Harris N, Shaik S (2001) J Am Chem Soc 123:3037. doi:10.1021/ja003544+
38. Hirao H, Kumar D, Thiel W, Shaik S (2005) J Am Chem Soc 127:13007. doi:10.1021/ja053847+
39. Ekroos M, Sjögren T (2006) Proc Natl Acad Sci USA 103:13682. doi:10.1073/pnas.0603236103
40. Becke AD (1988) Phys Rev A 38:3098. doi:10.1103/PhysRevA.38.3098
41. Becke AD (1993) J Chem Phys 98:5648. doi:10.1063/1.464913
42. Lee C, Yang W, Parr RG (1988) Phys Rev B Condens Matter 37:785. doi:10.1103/PhysRevB.37.785
43. Frisch MJ, Trucks GW, Schlegel HB, Scuseria GE, Robb MA, Cheeseman JR, Montgomery JJA, Vreven T, Kudin KN, Burant JC, Millam JM, Iyengar SS, Tomasi J, Barone V, Mennucci B, Cossi M, Scalmani G, Rega N, Petersson GA, Nakatsuji H, Hada M, Ehara M, Toyota K, Fukuda R, Hasegawa J, Ishida M, Nakajima T, Honda Y, Kitao O, Nakai H, Klene M, Li X, Knox JE, Hratchian HP, Cross JB, Adamo C, Jaramillo J, Gomperts R, Stratmann RE, Yazyev O, Austin AJ, Cammi R, Pomelli C, Ochterski JW, Ayala PY, Morokuma K, Voth GA, Salvador P, Dannenberg JJ, Zakrzewski VG, Dapprich S, Daniels AD, Strain MC, Farkas O, Malick DK, Rabuck AD, Raghavachari K, Foresman JB, Ortiz JV, Cui Q, Baboul AG, Clifford S, Cioslowski J, Stefanov BB, Liu G, Liashenko A, Piskorz P, Komaromi I, Martin RL, Fox DJ, Keith T, Al-Laham MA, Peng CY, Nanayakkara A, Challacombe M, Gill PMW, Johnson B, Chen W, Wong MW, Gonzalez C, Pople JA (2003) Gaussian03 b01. Gaussian Inc., Pittsburgh
44. Hay PJ, Wadt WR (1985) J Chem Phys 82:299. doi:10.1063/1.448975
45. Ditchfield R, Hehre WJ, Pople JA (1971) J Chem Phys 54:724. doi:10.1063/1.1674902
46. Hehre WJ, Ditchfield R, Pople JA (1972) J Chem Phys 56:2257. doi:10.1063/1.1677527
47. Francl MM, Pietro WJ, Hehre WJ, Binkley JS, DeFrees DJ, Pople JA et al (1982) J Chem Phys 77:3654. doi:10.1063/1.444267
48. Clark T, Chandrasekhar J, Spitznagel GW, Schleyer Pv R (1983) J Comput Chem 4:294. doi:10.1002/jcc.540040303
49. Frisch MJ, Pople JA, Binkley JS (1984) J Chem Phys 80:3265. doi:10.1063/1.447079
50. Wigner E (1932) Z Physik Chem Br 19:203
51. Skodje RT, Truhlar DG (1981) J Phys Chem 85:624. doi:10.1021/j150606a003
52. Skodje RT, Truhlar DG, Garrett BC (1981) J Phys Chem 85:3019. doi:10.1021/j150621a001
53. Filatov M, Shaik NHS (1999) Angew Chem Int Ed 38:3510. doi:10.1002/(SICI)1521-3773(19991203)38:23<3510::AID-ANIE3510>3.0.CO;2-#
54. Hammond GS (1955) J Am Chem Soc 77:334. doi:10.1021/ja01607a027
55. Krauser JA, Guengerich FP (2005) J Biol Chem 280:19496. doi:10.1074/jbc.M501854200
56. Truhlar DG, Garrett BC, Klippenstein SJ (1996) J Phys Chem 100:12771. doi:10.1021/jp953748q
57. Miller WH, Handy NC, Adams JE (1980) J Chem Phys 72:99. doi:10.1063/1.438959
58. Truhlar DG, Gordon MS (1990) Science 249:491. doi:10.1126/science.249.4968.491
59. Kim Y, Corchado JC, Villa J, Xing J, Truhlar DG (2000) J Chem Phys 112:2718. doi:10.1063/1.480846
60. Albu TV, Corchado JC, Truhlar DG (2001) J Phys Chem A 105:8465. doi:10.1021/jp011951h
61. Truhlar DG (2002) J Phys Chem A 106:5048. doi:10.1021/jp0143342
62. Lin H, Pu JZ, Albu TV, Truhlar DG (2004) J Phys Chem A 108:4112. doi:10.1021/jp049972+
63. Kim KH, Kim Y (2004) J Chem Phys 120:623. doi:10.1063/1.1630305
64. Lin H, Zhao Y, Tishchenko O, Truhlar DG (2006) J Chem Theory Comput 2:1237. doi:10.1021/ct600171u
65. Tishchenko O, Truhlar DG (2006) J Phys Chem A 110:13530. doi:10.1021/jp0640833
66. Higashi M, Truhlar DG (2008) J Chem Theory Comput 4:790. doi:10.1021/ct800004y
67. Ogliaro F, Cohen S, de Visser SP, Shaik S (2000) J Am Chem Soc 122:12892. doi:10.1021/ja005619f
68. Altun A, Shaik S, Thiel W (2006) J Comput Chem 27:1324. doi:10.1002/jcc.20398
69. Yano JK, Wester MR, Schoch GA, Griffin KJ, Stout CD, Johnson EF (2004) J Biol Chem 279:38091. doi:10.1074/jbc.C400293200
70. Williams PA, Cosme J, Vinkovic DM, Ward A, Angove HC, Day PJ et al (2004) Science 305:683. doi:10.1126/science.1099736
71. de Visser SP, Kumar D, Cohen S, Shacham R, Shaik S (2004) J Am Chem Soc 126:8362. doi:10.1021/ja048528h
72. Olsen L, Rydberg P, Rod TH, Ryde U (2006) J Med Chem 49:6489. doi:10.1021/jm060551l
73. Singh SB, Shen LQ, Walker MJ, Sheridan RP (2003) J Med Chem 46:1330. doi:10.1021/jm020400s
74. Korzekwa KR, Jones JP, Gillette JR (1990) J Am Chem Soc 112:7042. doi:10.1021/ja00175a040